GEOPHYSICS, VOL. 72, NO. 2 (MARCH-APRIL 2007); P. P23–P31, 12 FIGS.
10.1190/1.2428268

Instantaneous spectral attributes to detect channels

Jianlei Liu[1] and Kurt J. Marfurt[2]

ABSTRACT

Channels filled with porous rock and encased in a nonporous matrix constitute one of the more important stratigraphic exploration plays. Although attributes such as coherence can be used to map channel width, they are relatively insensitive to channel thickness. In contrast, spectral decomposition can be used to map subtle changes in channel thickness. The peak spectral frequency derived by using the short-window, discrete Fourier transform (SWDFT) is an excellent tool for mapping such changes along an interpreted horizon. We show that by use of instantaneous spectral attributes, we can generate equivalent maps for complete seismic volumes. Because we are often interested in mapping high-reflectivity channels encased in a lower-reflectivity matrix, we find that a composite plot of the peak frequency and the above-average peak amplitude accentuates highly tuned channels. Finally, by generating a composite volume using peak frequency, peak amplitude, and coherence, we can establish not only the channel thickness, but also its width. We demonstrate the value of such 3D volumetric estimates through application to (1) a marine survey acquired over Tertiary channels from the Gulf of Mexico and (2) a land data survey acquired over Paleozoic channels from the Central Basin Platform, west Texas, United States. The channels in both marine and land surveys can be highlighted through composite-volume analysis.

INTRODUCTION

Channels filled with porous rock and encased in a nonporous matrix constitute one of the more important stratigraphic exploration plays. However, detailed mapping of channels has a much broader impact. By using modern and paleoanalogues, mapping channels helps us to understand the paleodepositional environment and thereby permits us to interpret less obvious prospective areas such as fans and levees. By mapping the width, tortuosity, and spatial relationship of meandering channels, avulsions, and braided streams, among other features, geomorphologists are able to infer channel depth and fluid velocity during the time of formation and thus better determine whether the fill is sand or shale prone.

Seismic coherence and other edge-sensitive attributes (Bahorich and Farmer, 1995; Luo et al., 2003) are among the most popular means of mapping channel boundaries. Although these attributes can easily detect channel edges, they cannot indicate the channel's thickness. In addition, as channels become very thin (well below one-quarter wavelength), their waveform becomes constant, such that coherence measures based on waveform shape cannot see the channel at all (Chopra and Marfurt, 2006).

From its inception, spectral decomposition has also been used to highlight channels (Partyka et al., 1999; Peyton et al., 1998). The spectral-decomposition images are complementary to coherence and edge-detection attribute images in that they are sensitive to channel thickness rather than to lateral changes in seismic waveform or amplitude. Initially, spectral-decomposition analysis was done within a fixed-sized analysis window (by using a short-window, discrete Fourier transform (SWDFT)) following a picked stratigraphic horizon, thereby generating a suite of constant-frequency spectral-amplitude maps. Most commonly, the interpreter animates through the maps and chooses the ones whose spatial pattern corresponds to a reasonable geologic model. Specifically, there is a strong correlation between channel thickness and spectral amplitude (Laughlin et al., 2002).

Widess (1973) shows that for thin beds below the tuning thickness, the composite seismic amplitude decreases linearly with thickness. Chuang and Lawton (1995) generalizes this work to a frequency spectrum and observed that the peak frequency slightly increases as the layer thickness decreases. Marfurt and Kirlin (2001) exploit this observation and apply it to an SWDFT over the Pliocene-Pleistocene deposits of the Mississippi River in the Gulf of Mexico. They found that the frequency corresponding to the peak spectral

Manuscript received by the Editor February 23, 2006; revised manuscript received September 28, 2006; published online January 22, 2007.
[1]Formerly University of Houston, Center for Applied Geosciences and Energy, Houston, Texas; presently Chevron Energy Technology Company, Houston, Texas. E-mail: jianlei.liu@chevron.com.
[2]University of Houston, Department of Geosciences, Houston, Texas. E-mail: kmarfurt@uh.edu.

amplitude is an excellent means of summarizing the information content of the full spectrum: a low-peak frequency corresponds to thick channels, and a high-peak frequency corresponds to thin channels.

Even with careful tapering, spectral decomposition using the SWDFT has window effects (Cohen, 1995). For this reason, Castagna et al. (2003) looked at alternative methods for time-frequency decomposition based on wavelet transforms to compute what is commonly called instantaneous spectral attributes (ISA). Much of this work has been used to identify channels (e.g., Sinha et al., 2005; Matos et al., 2005), but to our knowledge, little has been published on the use of peak-frequency volumes based on these techniques, although Liu et al. (2004) showed how the ISA peak frequency significantly increases with decreasing layer thickness.

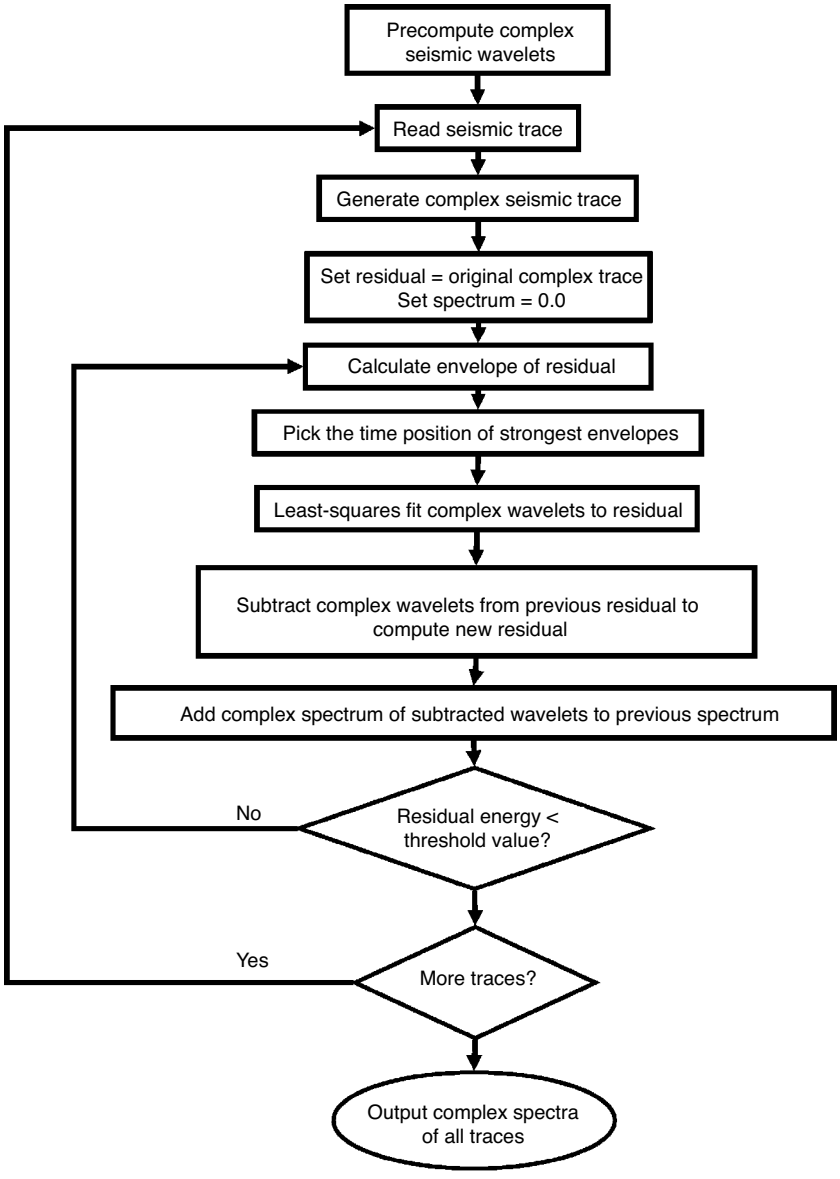

Figure 1. A flowchart for a wavelet-based spectral-decomposition algorithm using a matching-pursuit technique. Typically we precompute a complex wavelet dictionary at intervals of 0.5 Hz.

In this paper, we show how spectral decomposition can be used to generate complete volumes of both peak spectral frequency and the amplitude at that peak spectral frequency. We begin by reviewing how we compute ISA components by using a matching-pursuit algorithm. Because we are interested in lateral changes in tuning associated with channels, rather than absolute spectral amplitudes, we introduce the peak spectral amplitude above the average spectral amplitude at each analysis point. Next, we show how these algorithms behave on simple synthetics. We then show how the peak frequency and the amplitude of the peak frequency can be effectively corendered through the use of a 2D color map (or palette). By generating a composite of this 2D color map with a gray scale, we can also corender coherence. Finally, we apply this workflow to two channels systems: the first seen in a marine survey over Tertiary channels acquired in the Gulf of Mexico and the second seen in a land survey over Paleozoic channels acquired in the Central Basin Platform, west Texas, United States.

ALGORITHM DESCRIPTION

We decompose the data by using a matching-pursuit wavelet-based spectral-decomposition algorithm shown in Figure 1 and presented by Liu and Marfurt (2005). The details of the algorithm description can be found in Appendix A. We begin by calculating the instantaneous envelope and frequency for each input trace. We then identify key seismic events by picking a suite of envelope peaks that fall above a user-specified percentage of the largest peak in the current (residual) trace. We have found that this implementation converges faster and provides a more-balanced spectrum of interfering thin beds than the alternative "greedy" matching-pursuit implementation (Mallat and Zhang, 1993) that fits the wavelet having the largest envelope, one at a time. The peak frequency of the wavelet can be approximately calculated by the instantaneous frequency of the residual trace at the envelope peak (Robertson and Nogami, 1984). The amplitudes and phases of each of the selected wavelets are computed together by using a simple least-squares algorithm. Each picked event has a corresponding wavelet. We compute the complex spectrum of the modeled trace by simply adding the complex spectrum of each constituent wavelet. This process is repeated until the residual falls below a desired threshold. In spite of our original work using the popular Morlet wavelets (Liu and Marfurt, 2005), we have found that a Ricker wavelet basis function proposed by Liu et al. (2004) better fits seismic data that tend to be biased toward the lower frequencies.

To better illustrate the flow shown in Figure 1, we apply it to a seismic line extracted from a 3D

survey acquired over the Central Basin Platform. The amplitude and time of the chosen waveletsare displayed in Figure 2d. At each iteration, we generate the corresponding seismic wavelets and add them to the previously modeled data (Figure 2a), compute a new data residual (unmodeled data) (Figure 2b), and accumulate the complex spectrum, of which we display the 40-Hz component in Figure 2c.

If the seismic data have not been previously spectrally balanced, it is common practice to do so within the spectral-decomposition algorithm. Following Partyka et al. (1999), we assume the geology to be random over a suite of neighboring time slices, giving rise to an underlying "white" reflectivity spectrum. We then balance the spectrum within a user-defined bandwidth as shown in Figure 3. Spectral balancing accounts for changes in the source wavelet with depth. The average spectrum over the entire survey at a given time before balancing is shown in Figure 3a. The balanced average spectrum is demonstrated in Figure 3b. If we define the average spectrum as $\langle \alpha(f) \rangle$, which is a function of frequency f, and its maximum as α_{max}, we estimate a noise level as a fraction ε of the peak spectral amplitude. Then we rescale each spectral component by $1/[\langle \alpha(f) \rangle + \varepsilon \cdot \alpha_{max}]$ thereby obtaining a "balanced" average spectrum. Some workers find that balancing the median rather than the mean spectrum provides better results in the presence of bright spots (G. A. Partyka, personal communication, 2005). For our two examples, the mean and median spectra are nearly identical. Such spectral balancing is important in extracting tuning effects (such as the peak spectral frequency) of the geology, in order not to be biased toward the spectral behavior of the seismic wavelet.

Once balanced, we can animate through time or horizon slices of discrete spectral components, interpret selected volumes of discrete spectral components, or generate composite volumes of peak frequency, peak amplitude, and coherence attributes. Peak amplitude is the maximum magnitude of the amplitude spectrum. And peak frequency is the frequency at the peak amplitude.

SYNTHETIC MODEL

A simple 1D synthetic seismic trace is shown in Figure 4a. The source wavelets are Morlet wavelets with peak frequency at 10 Hz, 30 Hz, and 50 Hz. The Morlet wavelets with 10-Hz peak frequency have 0° phase. The Morlet wavelets with 50-Hz peak frequency have 90° phase. The phases of Morlet wavelets with 30-Hz peak frequency are 0° and 45°. Figure 4b demonstrates the final time-frequency distribution plot of Figure 4a. The time extension of the time-frequency distribution is constrained by the en-

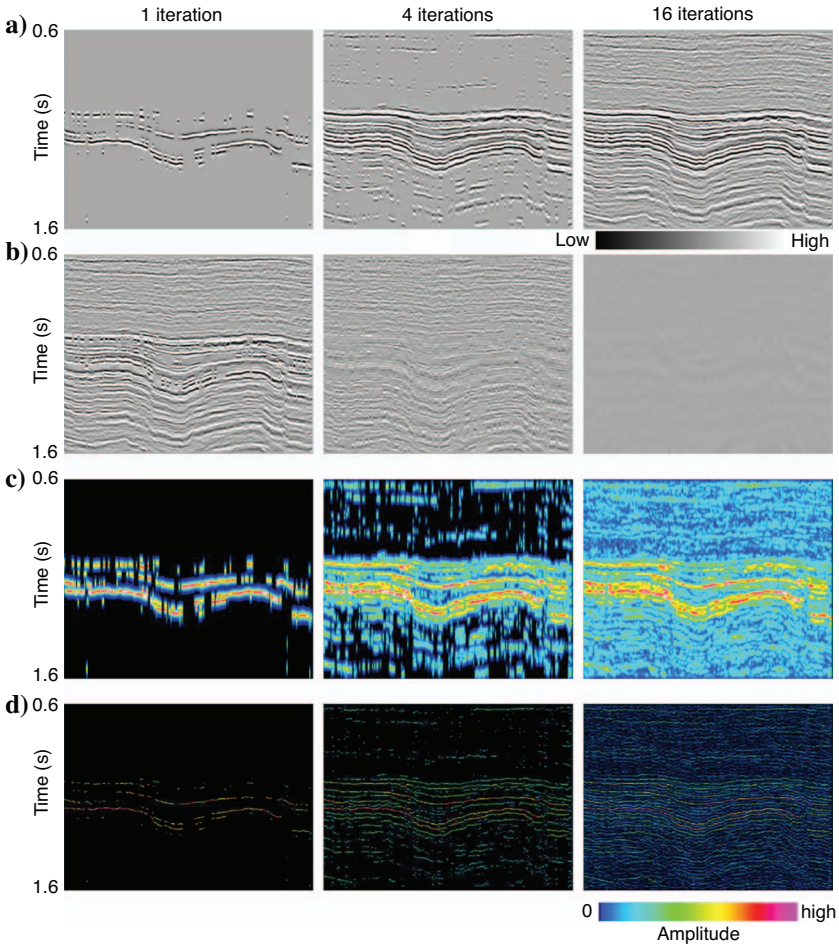

Figure 2. Illustration of the matching-pursuit algorithm described in Figure 1 applied to a survey acquired over the Central Basin Platform. Columns represent algorithm results after the first, fourth, and 16th iteration of (a) modeled data, (b) residual (unmodeled) data, (c) the 40-Hz component of the modeled data, and (d) the wavelet location and envelope of the modeled data. The frequency and phase of the modeled data are not displayed. Data are courtesy of Burlington Resources.

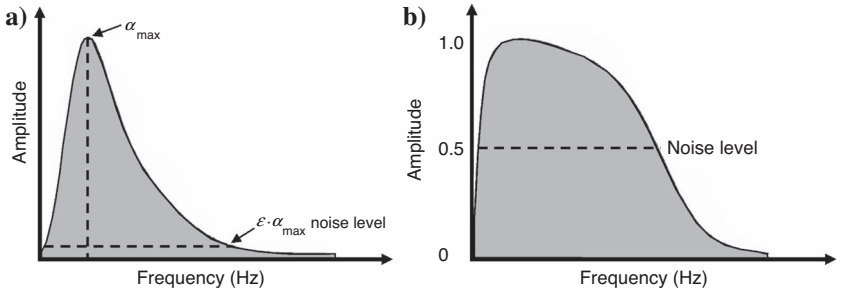

Figure 3. Spectral balancing to account for changes in the source wavelet with depth (rescale each spectral component by $1/[\langle \alpha(f) \rangle + \varepsilon \cdot \alpha_{max}]$). (a) The average spectrum before balancing. (b) The average spectrum after balancing.

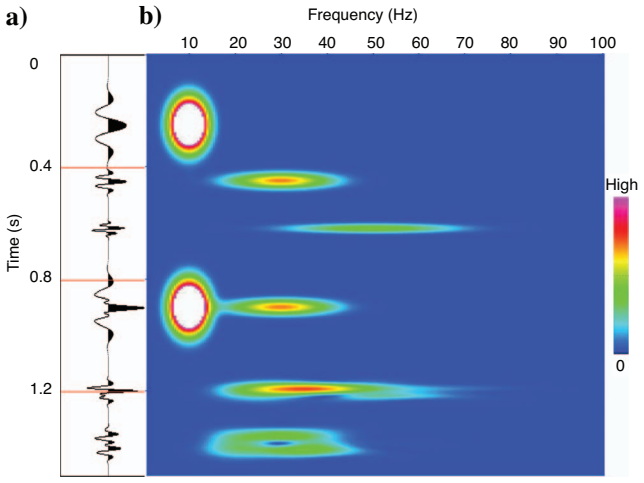

Figure 4. (a) A simple 1D synthetic seismic trace that is composed of different Morlet wavelets. (b) Time-frequency distribution plot of (a).

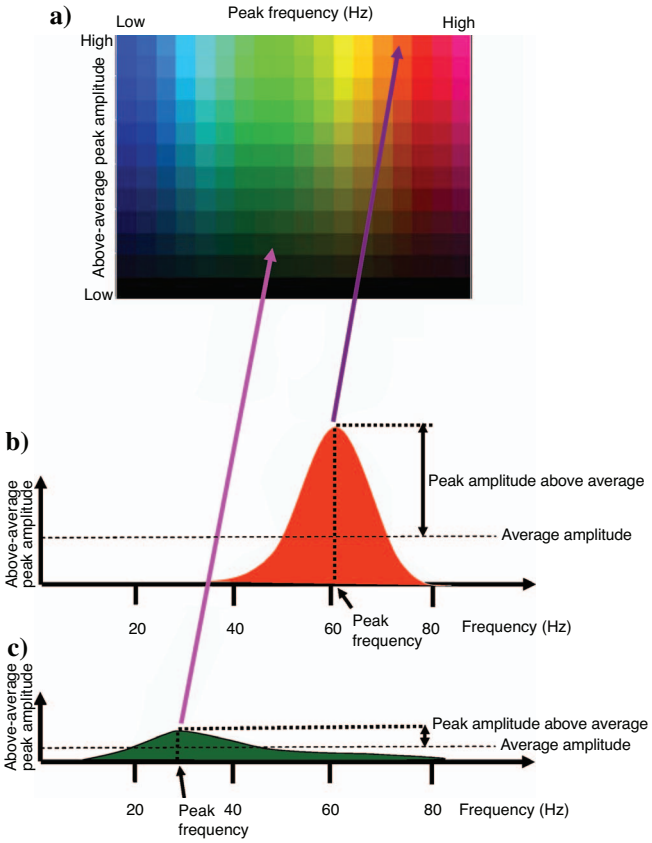

Figure 5. (a) A 2D color chart of peak frequency (hue) and peak amplitude above background (lightness) (as shown in Lin et al., 2003). (b and c) Two idealized spectra: (b) A spectrum with a high peak frequency and high above-average peak amplitude maps to a bright orange color, and (c) a spectrum with a low peak frequency and only average peak amplitude maps to a dark green color.

velope of matched wavelets. We can easily see that the low-frequency wavelet has a longer time spreading, whereas the high-frequency wavelet has a shorter time extension, but has greater bandwidth.

2D COLOR CHART

Many seismic attributes are only meaningful when put in the context of a second, independent, attribute. For example, a measurement of reflector azimuth is meaningless if the dip magnitude of the reflector is flat. Similarly, a measure of wavelet phase is meaningless if its amplitude falls below the signal-to-noise level. In this paper, the value of the peak spectral frequency has meaning only if that peak lies significantly above the average spectrum. We use a 2D color map that combines hue and lightness to represent peak frequency and above-average peak amplitude, respectively (Figure 5a), and two idealized spectra (Figure 5b and c), one that is high amplitude, highly peaked at a high frequency, and one that is lower amplitude, flatter, and peaked at a lower frequency. Because the spectrum shown in Figure 5b has a relatively higher peak frequency and above-average peak amplitude, it is represented by the bright orange color shown in Figure 5a. In contrast, the spectrum shown in Figure 5c has a lower peak frequency and only an average peak amplitude and is represented by the dark green color shown in Figure 5a.

To display coherence, we turn to the concept of composite displays discussed by Chopra (2001) and Lin et al. (2003). In this paper, if the coherence is above a threshold, we display the peak frequency and amplitude through the use of the 2D color table displayed in Figure 5a. If the coherence falls below a threshold, we display the coherence against a 1D gray scale. In this manner, coherence defines the edges (and thus width) of the channels, and the peak frequency defines the relative thickness.

EXAMPLES FROM FIELD DATA

A marine survey over Tertiary channels: South Marsh Island, Gulf of Mexico

Conventional analysis through animation of spectral components as described by Partyka et al. (1999) works very well when applied to a horizon. This methodology breaks down, however, when analyzing volumes of seismic data. Generation of 80 output volumes at 1-Hz increments between 10 and 90 Hz quickly fills all the disk space available. The computational effort of spectral decomposition is greatly outweighed by the shear amount of output data. Even though we can reduce the output volumes by sampling every 10 Hz, it is still awkward to simultaneously deal with nine common-frequency volumes. For this reason, we propose initially generating only the peak frequency and peak amplitude volumes by time-frequency decomposition, and combining them with coherence, thereby providing an image that can be used to rapidly identify features of stratigraphic interest. If appropriate, the individual spectral components can be regenerated and examined either along constrained zones of interest or for a constrained range of frequencies (such as done for reservoir illumination by Fahmy et al., 2005). A composite volume of peak frequency, peak amplitude, and coherence is created in the following examples.

Figure 6a shows the time slice of the coherence volume at t = 1.416 s. White arrows indicate a wide main channel, and yellow arrows indicate a narrow branch channel. In the time slice through the 20-Hz spectral component (Figure 6b), only the main channel shows up. In contrast, in the time slice through the 60-Hz spectral component (Figure 6c), only the branch channel shows up. This phenomenon implies that the main channel is thicker than its branch.

Figure 7a shows the time slice of the coherence volume at t = 1.230 s. The meandering channels are easily interpreted in the coherence volume (white arrows). Figure 7b demonstrates the composite volume of peak frequency, peak amplitude, and coherence of the same time. In Figure 7b, white arrows point to the meandering channels. Compared to the gray image in Figure 7a, the composite plot (including hue, lightness, and gray) in Figure 7b better distinguishes the channels from the background. For instance, most of the channels appear as green. The coherence can detect the discontinuity of seismic events (which means the coherence volume can detect the edge of the channel), whereas the peak frequency and peak amplitude allow the channel to be highlighted in a distinctive color.

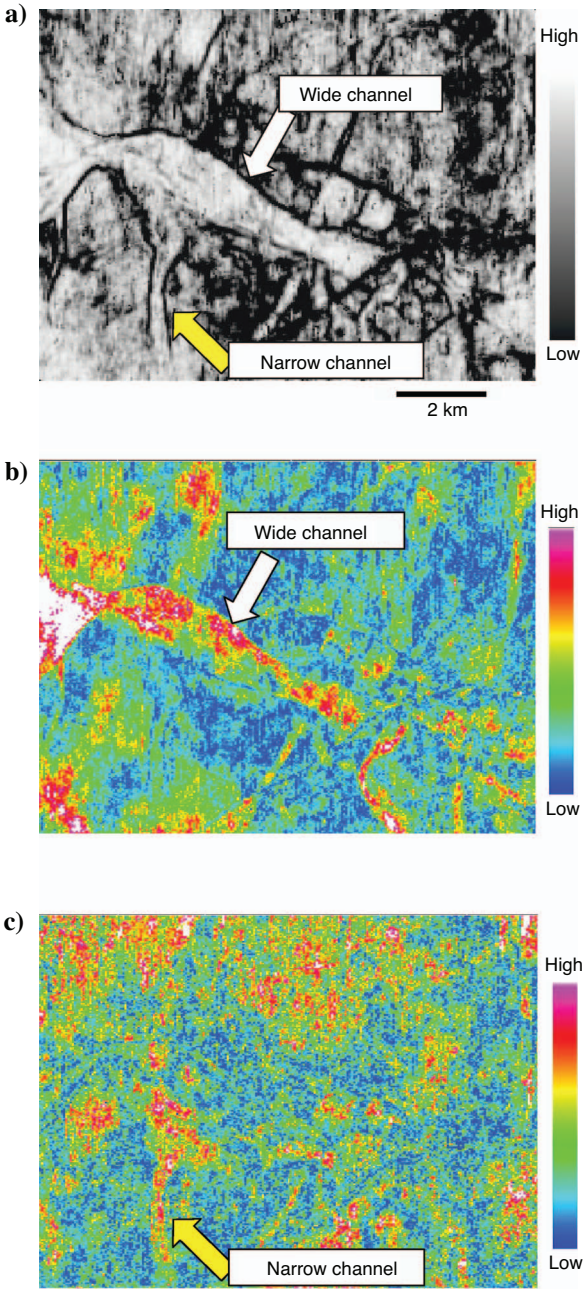

Figure 6. Time slices at t = 1.416 s through a survey acquired over Tertiary channels, South Marsh Island, Gulf of Mexico, showing (a) coherence, (b) the 20-Hz spectral component, and (c) the 60-Hz spectral component. (Horizontal and vertical scales are the same.)

A land survey over Paleozoic channels: Central Basin Platform, west Texas, United States

We now apply this same technique to older indurated rocks imaged in a field-data example from west Texas to illustrate the spectral-decomposition technique in Figure 2. Figure 8 shows the time slice of seismic volume at t = 1.060 s. The arrows point to Pennsylvanian channel deposits. Figures 9 and 10 show two time slices at t = 1.060 s and 1.096 s of peak frequency and above-average peak amplitude (peak amplitude minus average amplitude value) through the use of the 2D color chart shown in Figure 5a. The channels are

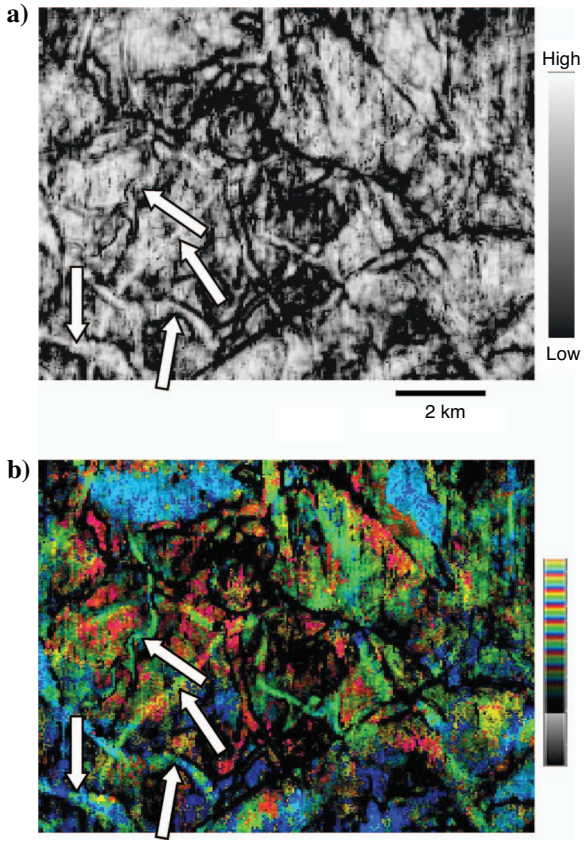

Figure 7. Time slices at t = 1.230 s through a survey acquired over Tertiary channels, South Marsh Island, Gulf of Mexico, showing (a) coherence volume and (b) composite volume of peak frequency, peak amplitude, and coherence. (Horizontal and vertical scales are the same.)

clearly shown in these two time slices. We note that the channel has a green color whereas the background has blue color, implying that the channel has a higher peak frequency than the background response. In these images, we did not use coherence to identify the edges of the channel, so the color green itself highlights the channels. To view all the channels in one slice, we flatten the volume along the unconformity horizon (the blue pick shown in Figure 12a). Figure 11a shows the phantom-horizon slice 44 ms above the unconformity. The accompanying amplitude spectra (Figure 11b-d) correspond to the points indicated by the magenta arrows. Figure 11b shows a peak frequency at about 62 Hz and high above-average peak amplitude; the plot points to an area that is thus mapped as bright yellow in Figure 11a. Figure 11c shows a peak frequency at about 50 Hz and moderate above-average peak amplitude; the plot points to the channelthat is mapped as light green in Figure 11a. Figure 11d shows a peak frequency at about 16 Hz and moderate above-average peak amplitude; these characteristics indicate a background response, and the area is mapped as a light blue in Figure 11a.

Figure 12a shows the seismic section of line AB from Figure 11a, and the same amplitude spectra as in Figure 11 are shown in Figure 12b-d. In the seismic section, we see that the notches in Figure 12b are cause by bed interferences. Figure 12c corresponds to the amplitude spectrum of a channel's response, which shows a relatively higher peak frequency compared to the background response of Figure 12d. Bed interferences can cause frequency notches (which depend on bed thickness and geometry); some of these can be individually resolved (as in Figure 12b) but others cannot (Figure 12c).

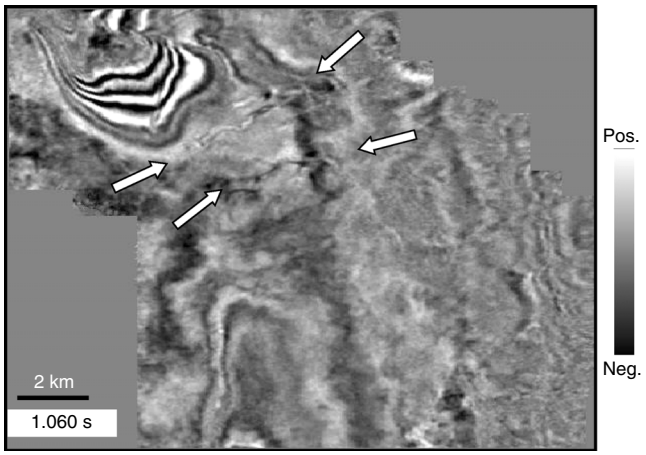

Figure 8. Time slice of the seismic volume at t = 1.060 s through a survey acquired over the Central Basin Platform. The survey is also used in Figure 2. White arrows point to two different channel branches. (Seismic data courtesy of Burlington Resources.)

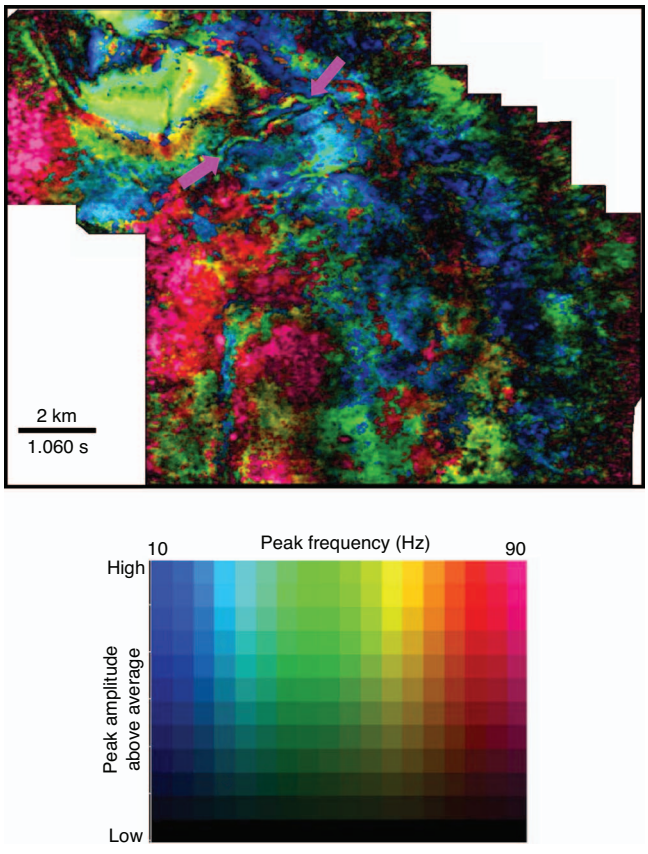

Figure 9. Time slice of the composite volume of peak frequency and above-average peak amplitude at t = 1.060 s. (Magenta arrows point to channel.) Colors are as in the 2D color chart in Figure 5a.

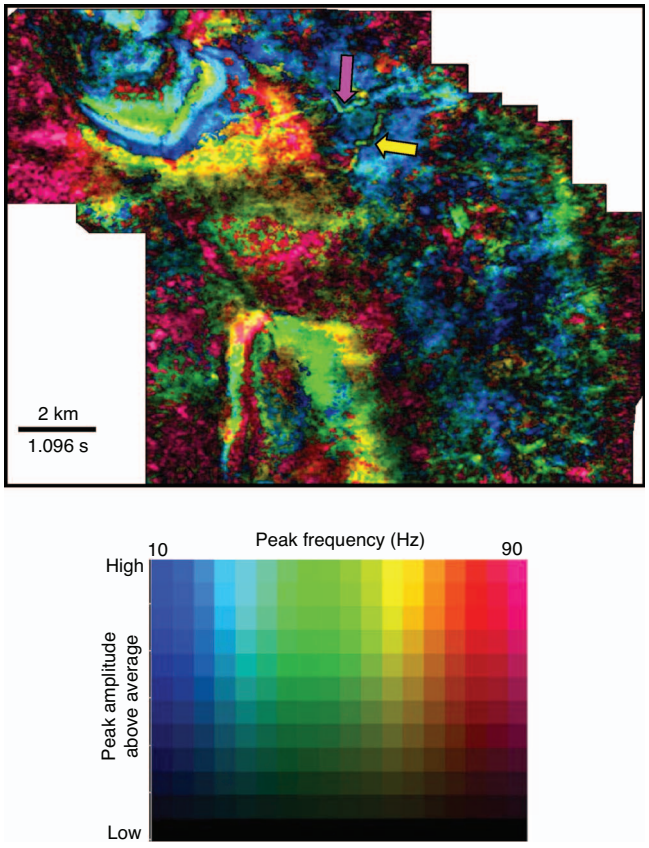

Figure 10. Time slice of the composite volume of peak frequency and above-average peak amplitude at t = 1.096 s. (Magenta and yellow arrows point to channels.) Colors are as in the 2D color chart in Figure 5a.

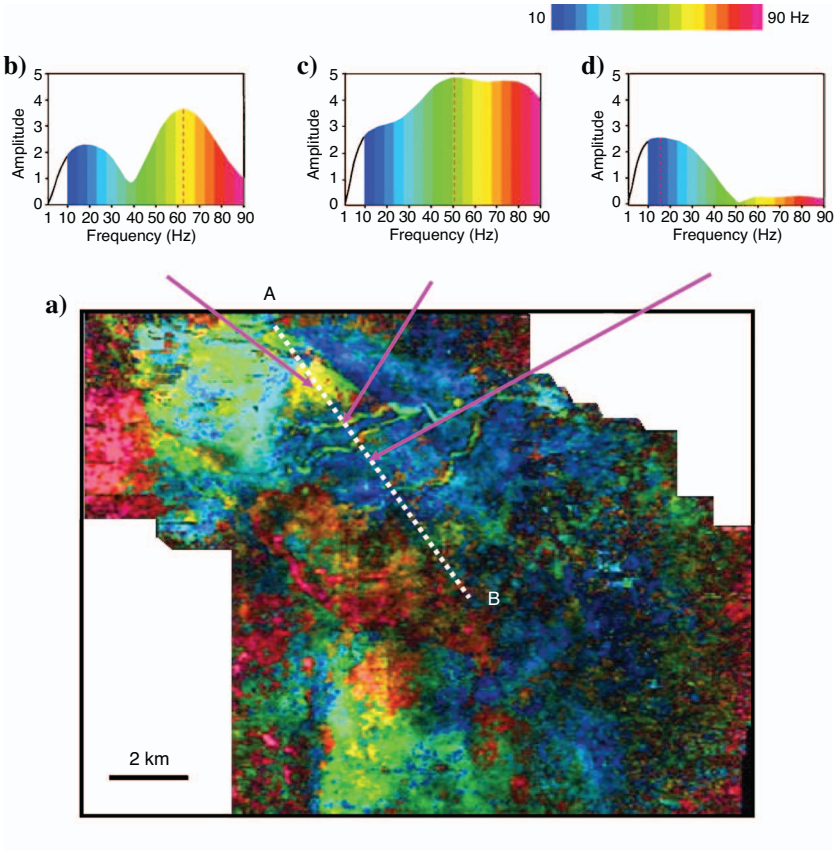

Figure 11. (a) Phantom-horizon slice 44 ms above the unconformity through a composite volume of peak frequency, above-average peak amplitude, and coherence using the technique described in Figure 5. (b) Amplitude spectrum of the erosional unconformity, which appears as bright yellow. (c) Amplitude spectrum of the Pennsylvanian channels draining the erosional unconformity, which appears as bright green. (d) Amplitude spectrum of channel matrix, which appears as a lower-amplitude spectrum and thus is dark blue.

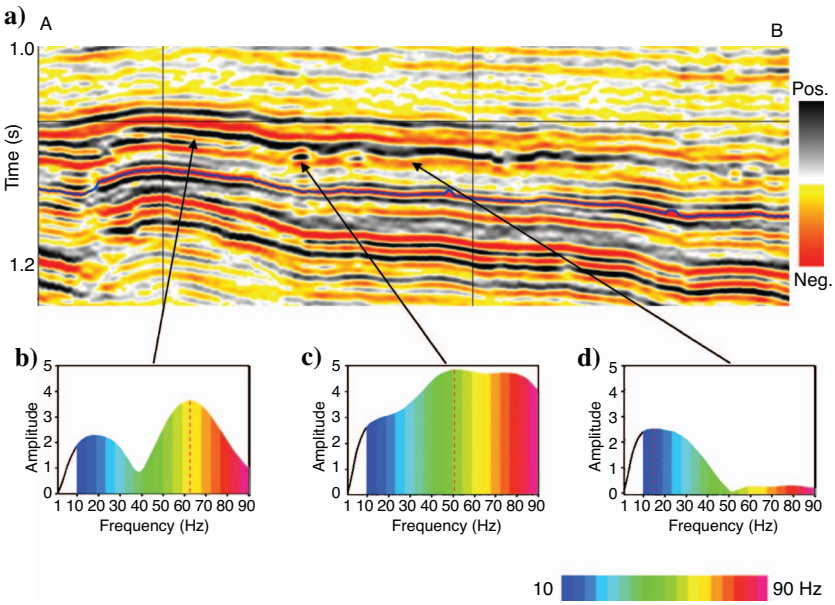

Figure 12. (a) Seismic section of line AB from Figure 11. (b–d) The same amplitude spectra as Figure 11. (Blue line indicates unconformity.)

At present, we interpret these images in three steps. First we use principles of geomorphology, together with modern and paleoanalogues, to identify stratigraphic features of interest. Second, we calibrate these patterns through conventional interpretation of the vertical seismic section, coupled with our understanding of the physics of thin-bed interference phenomena. Finally, we use the colors to provide a quantitative estimate of relative channel thickness, and we use coherence to provide a qualitative estimate of channel width. These tools allow us to unravel stratigraphic features of interest preserved in the geologic record.

CONCLUSIONS

We propose a new spectral-decomposition method that combines the concept of matching-pursuit and least-squares solution. Through the use of instantaneous spectral analysis derived from wavelet-based spectral decomposition, we have extended the concept of using peak spectral frequency of mapped horizons to full 3D volumes. We find that these peak spectral frequencies are most useful if modulated by some measure of the corresponding spectral amplitude. For channels where we expect lateral changes in thin-bed tuning, we find that the peak spectral amplitude above the average spectral amplitude is particularly useful by deemphasizing the appearance of strong-amplitude flat spectral responses.

Although spectral decomposition is a good indicator of channel thickness, coherence and other edge detectors are good indicators of channel width. For this reason, we advocate displaying both attributes in a composite image. We have shown the effectiveness of this technique in mapping Tertiary channels in a marine survey. We find this technique to be an excellent tool for rapidly mapping channels that may be of importance both for prospect evaluation and for quantifying reservoir heterogeneity. We are encouraged to think that by using these three measures together, we can develop improved geostatistics or neural network flows that, with well control, can help us quantitatively estimate reservoir thickness.

ACKNOWLEDGMENTS

We thank the sponsors of Allied Geophysical Laboratories at the University of Houston and the CRC Petroleum Research Fund for their support of this research effort. We give special thanks to Charlotte Sullivan, Fred Hilterman, and John Castagna for their helpful feedback. We also thank Fairfield Industries and Burlington Resources for providing the field data. Finally, we

thank the associate editor of *Geophysics* and two anonymous reviewers for their valuable comments and suggestions.

APPENDIX A

MATCHING-PURSUIT SPECTRAL ANALYSIS

We begin our analysis by assuming that each seismic time trace, $u(t)$, is band limited and can be represented by a linear combination of either Ricker or Morlet wavelets:

$$u(t) = \sum_j a_j \cdot w(t - t_j, f_j, \varphi_j) + \text{Noise}, \qquad \text{(A-1)}$$

where a_j, t_j, f_j, and φ_j represent the amplitude, center time, peak frequency, and phase of the jth wavelet. We exploit complex attribute analysis and estimate the center time of each candidate wavelet by peaks in the instantaneous envelope. We estimate the average frequency f_{avg} of the wavelet by the instantaneous frequency at the envelope peak [called *response frequency* by Bodine (1984) and *wavelet frequency* by Taner (2000)]. The peak frequency f_j shown in equation A-1 can be computed for the Ricker wavelet by

$$f_j = (\sqrt{\pi}/2) f_{\text{avg}}, \qquad \text{(A-2)}$$

and for the Morlet wavelet by

$$f_j = f_{\text{avg}}. \qquad \text{(A-3)}$$

The temporal behavior of the Ricker wavelet is given by

$$w_R(t, f_j) = (1 - 2\pi^2 f_j^2 t^2)\exp(-\pi^2 t^2 f_j^2), \qquad \text{(A-4)}$$

and its spectrum is given by

$$\bar{w}_R(f, f_j) = \frac{2}{\sqrt{\pi}} \frac{f^2}{f_j^3} \exp\left(-\frac{f^2}{f_j^2}\right). \qquad \text{(A-5)}$$

The temporal behavior of the Morlet wavelet is given by

$$w_M(t, f_j) = \exp(-t^2 f_j^2 \cdot \ln 2/k) \cdot \exp(i 2\pi f_j t), \qquad \text{(A-6)}$$

and its spectrum is given by

$$\bar{w}_M(f, f_j) = \frac{\sqrt{\pi/\ln 2}}{f_j} \cdot \exp\left[-k \cdot \frac{\pi^2 (f - f_j)^2}{\ln 2 \cdot f_j^2}\right], \qquad \text{(A-7)}$$

where f_j is the peak frequency, and k is a constant value that controls the wavelet breadth. If we use smaller values of k, we will include more cycles in the Morlet wavelet. In our process, we choose $k = 0.5$.

To efficiently solve for both the amplitude and phase of each wavelet, we use the Hilbert transform to form both an analytic data trace

$$U(t) = u(t) + i u^H(t) \qquad \text{(A-8)}$$

and a table of analytic complex Ricker wavelets

$$W(t, f_j) = w(t, f_j) + i w^H(t, f_j), \qquad \text{(A-9)}$$

where w indicates symmetric cosine wavelets and w^{H} indicates antisymmetric sine wavelets. For the table of analytic complex Morlet wavelets, we use equation A-6 to generate Morlet wavelets.

The analytic analogue of equation A-1 then becomes

$$U(t) = \sum_j A_j \cdot W_j(t - t_j, f_j) + \text{Noise}, \qquad \text{(A-10)}$$

where the amplitude a_j in equation A-1 is represented by the magnitude of the complex amplitude A_j, and the phase φ_j is represented by the phase of A_j.

Our objective is to minimize the energy of the residual trace $R(t)$, defined as the difference between the seismic trace and the matched wavelets

$$R(t) = \left\{ U(t) - \sum_j^J [A_j \cdot W_j(t - t_j, f_j)] \right\}^2, \qquad \text{(A-11)}$$

where we recall that t_j and f_j are known and A_j is unknown. To estimate all wavelet coefficients in one iteration, we write equation A-11 in matrix form and simply solve the normal equations

$$\mathbf{A} = [\mathbf{W^H W} + \varepsilon \mathbf{I}]^{-1} \mathbf{W^H U}, \qquad \text{(A-12)}$$

where $\mathbf{W} = [W(t - t_1, f_1), W(t - t_2, f_2), \ldots, W(t - t_m, f_m)]$ is a vector of wavelets centered at each envelope peak, $\mathbf{A} = (A_1, A_2, \ldots A_m)^{\text{T}}$ is a vector of complex wavelet amplitudes, $\mathbf{I}$ is the identity matrix, and ε is a small number that makes the solution stable.

In the matching-pursuit approach, we begin by fitting those wavelets corresponding to the largest wavelets' envelope first. In our application, we have chosen to fit those wavelets whose envelopes are greater than 50 % of the value of the largest event of the current trace (the original trace for the first iteration; the current residual for all subsequent residuals). We then follow the flow chart described in Figure 1 until the residual energy is acceptable.

Using equation A-5 or A-7 we compute the complex spectrum by summing the complex spectra of the constituent wavelets

$$\bar{u}(t, f) = \sum_{j=1}^{J} A_j \cdot \bar{w}_j(f, f_j) \text{env}[w(t - t_j, f_j)] e^{i 2\pi f (t - t_j)}, \qquad \text{(A-13)}$$

where

$$\text{env}[w(t - t_j, f_j)] = \{[w^2(t - t_j, f_j) + [w^H(t - t_j, f_j)]^2\}^{1/2} \qquad \text{(A-14)}$$

is the envelope of the complex wavelets. The amplitude spectrum is thus simply the magnitude of equation A-13, and the phase is the angle between its real and imaginary parts. We assume the wavelet spectra to be mathematically supported by the time duration of the seismic wavelets. If we wish to accurately reconstruct the amplitude of the original data from these complex spectra, we weight them by a boxcar function, giving rise to a rather blocky vertical section. We find that for interpretation purposes, it is more useful to weight the complex spectra by the envelope of the wavelets. Within this weighting window, the spectra must be phase shifted according to the sample time delay or advance from the envelope peak (equation A-14).

REFERENCES

Bahorich, M., and S. Farmer, 1995, 3D seismic discontinuity for faults and stratigraphic features: The coherence cube: The Leading Edge, **14**, 1053–1058.

Bodine, J. H., 1984, Waveform analysis with seismic attributes: 54th Annual International Meeting, SEG, Expanded Abstracts, 505–509.

Castagna, J., S. Sun, and R. Siegfried, 2003, Instantaneous spectral analysis: Detection of low-frequency shadows associated with hydrocarbons: The Leading Edge, **22**, 120–127.

Chopra, S., 2001, Adding the coherence dimension to 3D seismic data: Canadian Society of Exploration Geophysicists Recorder, **26**, 5–8.

Chopra, S., and K. J. Marfurt, 2006, Seismic attribute mapping of structure and stratigraphy: SEG.

Chuang, H., and D. C. Lawton, 1995, Frequency characteristics of seismic reflections from thin beds: Canadian Journal of Exploration Geophysics, **31**, 32–37.

Cohen, L., 1995, Time frequency analysis: Prentice-Hall, Inc.

Fahmy, W. A., G. Matteucci, D. Butters, and J. Zhang, 2005, Successful application of spectral decomposition technology toward drilling of a key offshore development well: 75th Annual International Meeting, SEG, Expanded Abstracts, 262–264.

Laughlin, K., P. Garossino, and G. Partyka, 2002, Spectral decomposition applied to 3D: AAPG Explorer, **23**, no. 5, 28–31.

Lin, I., K. J. Marfurt, and O. Johnson, 2003, Mapping 3-D multiattribute data into HLS color space: Applications to Vinton dome, LA: 73rd Annual International Meeting, SEG, Expanded Abstracts, 1728–1731.

Liu, J., and K. J. Marfurt, 2005, Matching pursuit decomposition using Morlet wavelets: 75th Annual International Meeting, SEG, Expanded Abstracts, 786–789.

Liu, J., Y. Wu, D. Han, and X. Li, 2004, Time-frequency decomposition based on Ricker wavelet: 74th Annual International Meeting, SEG, Expanded Abstracts, 1937–1940.

Luo, Y., S. Al Dossary, M. Marhoon, and M. Alfaraj, 2003, Generalized Hilbert transform and its application in geophysics: The Leading Edge, **22**, 198–202.

Mallat, S., and Z. Zhang, 1993, Matching pursuit with time-frequency dictionaries: IEEE Transactions on Signal Processing, **41**, 3397–3415.

Marfurt, K. J., and R. L. Kirlin, 2001, Narrow-band spectral analysis and thin-bed tuning: Geophysics, **66**, 1274–1283.

Matos, M. C., P. Osorio, E. C. Mundim, and M. Moraces, 2005, Characterization of thin beds through joint time-frequency analysis applied to a turbidite reservoir in Campos Basin, Brazil: 75th Annual International Meeting, SEG, Expanded Abstracts, 1429–1432.

Partyka, G. A., J. Gridley, and J. Lopez, 1999, Interpretational applications of spectral decomposition in reservoir characterization: The Leading Edge, **18**, 353–360.

Peyton, L., R. Bottjer, and G. Partyka, 1998, Interpretation of incised valleys using new 3-D seismic techniques: A case history using spectral decomposition and coherency: The Leading Edge, **17**, 1294–1298.

Robertson, J. D., and H. H. Nogami, 1984, Complex seismic analysis of thin beds: Geophysics, **49**, 344–352.

Sinha, S., R. Routh, P. Anno, and J. Castagna, 2005, Spectral decomposition of seismic data with continuous-wavelet transform: Geophysics, **70**, no. 6, P19–P25.

Taner, M. T., 2000, Attributes revisited: Http://www.rocksolidimages.com/pdf/attrib_revisited.htm, accessed June 22, 2006.

Widess, M. B., 1973, How thin is a thin bed?: Geophysics, **38**, 1176–1180.